Impact of magnesium on the structure of aluminoborosilicate glasses: A solid-state NMR and Raman spectroscopy study

Nicolas Bisbrouck, Marco Bertani, Frédéric Angeli, Thibault Charpentier, Dominique de Ligny, Jean-marc Delaye, S. Gin, Matthieu Micoulaut

Received <day> <Month>, <year>; | Revised <day> <Month>, <year>; | Accepted <day> <Month>, <year>

DOI: xxx/xxxx

ARTICLE TYPE

Impact of Magnesium on the Structure of Aluminoborosilicate Glasses: A Solid-State NMR and Raman Spectroscopy Study

Nicolas Bisbrouck[1] | Marco Bertani[2] | Frédéric Angeli*[1] | Thibault Charpentier*[2] | Dominique de Ligny[3] | Jean-Marc Delaye[1] | Stéphane Gin[1] | Matthieu Micoulaut[4]

[1]CEA, DES, ISEC, DE2D, Université de Montpellier, Marcoule, France
[2]Université Paris-Saclay, CEA, CNRS, NIMBE, 91191 Gif Sur Yvette, France.
[3]Department of Materials Science and Engineering, University of Erlangen-Nürnberg, DE91058 Erlangen, Germany
[4]Sorbonne Université, Laboratoire de Physique Théorique de la Matière Condensée, CNRS UMR 7600, 4 Place Jussieu, 75252 Paris Cedex 05, France

Correspondence
Frédéric Angeli and Thibault Charpentier
Email: frederic.angeli@ceaf.fr and thibault.charpentier@cea.fr

Present Address
Marco Bertani : Department of Chemical and Geological Sciences, University of Modena and Reggio Emilia, via G.Campi 103, 41125, Modena, Italy

Abstract

Seven magnesium-containing aluminoborosilicate glasses, with three to five oxides, have been studied through comprehensive multi-nuclear solid-state NMR (^{11}B, ^{27}Al, ^{29}Si, ^{23}Na, ^{17}O and ^{25}Mg) and Raman spectroscopy. The progressive addition of cations and the substitution of sodium and calcium by magnesium illuminate the impact of magnesium on the glass structure. The proportion of tri-coordinated boron drastically increased with magnesium addition, demonstrating the poor charge-compensating capabilities of magnesium in tetrahedral boron units. Oxygen-17 NMR showed the formation of mixing sites containing both Na and Mg near non-bridging oxygen sites. Furthermore, a high magnesium content appears to result in the formation of two sub-networks (boron and silicon rich) with different polymerisation degrees as well as to promote the formation of high-coordination aluminium sites (Al[V] and Al[VI]). Finally, magnesium coordination ranging from four to six, with a mean value shifting from five to six along the series, suggests that magnesium might endorse an intermediate role in these glasses.

KEYWORDS:
magnesium-25, structure, Raman spectroscopy, borosilicate glass, nuclear magnetic resonance, oxygen-17

1 | INTRODUCTION

Magnesium oxide is a key component in geological silicate melts and can induce interesting properties in silicate glasses with applications in various fields, from medicine to technological systems[1]. As one of the most abundant cations in magma, the study of magnesium-containing silicate glasses is fundamental to understanding magma transport[2,3]. In bioactive glasses used for bone repair, magnesium appears to enhance crystallisation and apatite formation in the early stages, favouring contact with living tissues[4–7]. From a technological point of view, adding magnesium to glasses intrinsically changes their properties such as viscosity[8], glass transition temperature[4], mechanical properties[8–12] and chemical durability[13]. Furthermore, some of the vitrified high-level waste (HLW) from nuclear facilities in the UK (Magnox)[14–16] and France (AVM)[17,18] contains relatively high magnesium proportions (around 5.90wt% and between 2.5 and 7.5wt% respectively[17]).

The role and impact of magnesium on the glass structure and its interactions with other cations are not yet fully understood; they can vary greatly with the chemical composition of the glass[10,15]. To understand the macroscopic properties of glasses, specifically the impact of magnesium, we performed an in-depth and detailed structural analysis at the atomic scale of glasses with various compositions, from simple to more complex ones. Generally considered as a network modifier and/or a charge compensator, several studies suggest that magnesium might exhibit an intermediate-to-network-forming role[15,19–21]. These assumptions are mainly based on its coordination number, typically ranging from four to six, as

extracted from X-ray diffraction[22–25], neutron scattering[22,23] and Raman[26,27] spectroscopy measurements as well as using molecular dynamic (MD) and reverse Monte-Carlo (RMC) simulations[23–25].

Solid-state nuclear magnetic resonance (NMR) spectroscopy has proven to be a useful and effective tool for probing the local environment of atoms in glasses, providing insights into the intricacies of silicate oxide glassy systems[28–36]. The network connectivity (Q_n), non-bridging oxygens (NBO), and coordination number (CN) can be precisely evaluated by investigating every NMR-active nucleus found in these glass systems, typically ^{27}Al, ^{11}B, ^{29}Si, ^{23}Na, ^{25}Mg, ^{43}Ca and ^{17}O[10,37–41]. While each nucleus provides specific information on its local chemical and geometric environment, ^{17}O NMR spectra provide insight into the various possible environments in oxide glasses. To that end, the best approach is to synthesise glasses using a sol–gel process to ensure a homogeneous distribution of ^{17}O in the network[29]. ^{17}O NMR measurements allow the observation of peculiar phenomena, such as the presence of Ca–Na or La–Na mixing sites near NBO-rich regions[42,43], which implies an extended structural disorder due to the non-randomness of the alkali/alkali-earth distribution. Recent studies[34] showed that Mg–Na mixing sites might also occurs. It is also implied that increasing the magnesium content leads to greater structural changes around the NBO in the glasses.

For nuclei such as ^{29}Si, ^{27}Al, or ^{11}B, a decrease in chemical shift typically results from an increase in the coordination number. For ^{25}Mg, most studies on the subject have focused on crystalline phases, **melts** or very simple glasses[19,20,30,44,44–49]; therefore, there is a lack of ^{25}Mg NMR data, particularly for borosilicate glasses. Indeed measuring the NMR spectrum of ^{25}Mg is difficult because of its low natural **abundance** (10%) and low Larmor frequency. Moreover, ^{25}Mg exhibits high quadrupolar interactions which can severely broaden the NMR spectra, making it even harder to distinguish magnesium environments in terms of the coordination number. With a sufficiently high enrichment in ^{25}Mg and owing to the availability of higher fields (in this work, **17.6 T**), it is possible to overcome these difficulties. Magnesium coordination in glass spectra can be approximately determined from NMR shifts from a comparison with the NMR spectra of crystalline materials, such as spinel ($MgAl_2O_4$) and åkermanite ($Ca_2MgSi_2O_7$) for which the four-fold coordinated magnesium isotropic chemical shifts are 49 and 52 ppm[19]. In the boron-containing mineral grandidierite, the MgO_5 bipyramid has been reported to have an approximately 55 ppm isotropic chemical shift[50]. In silicates containing magnesium, a six-fold coordinated magnesium contribution is visible in the range of 5 to 14 ppm[19,51]. However, some parameters such as bond length[52–54] and bond angle[55] or the second-neighbours effect[28,55] can affect the isotropic chemical shift, making it difficult to clearly identify the coordination.

In addition to the complexity of the structural role of magnesium and its coordination number in glasses, its impact on other cations in the network has not yet been clearly explained. Several studies have demonstrated that increasing the magnesium content in glasses leads to a greater proportion of highly disrupted four-fold coordinated aluminium and the formation of five- and six-fold coordinated aluminium[10,32,38,56]. Additionally, in borosilicate glasses, it appears that a relative increase in magnesium concentration compared to that of boron leads to an increase in three-fold coordinated boron that is greater than the effect of calcium[14,15,56–58]. It is suggested that this effect can be attributed to the greater mean field strength (MFS), defined as the charge over the squared cation-oxygen distance, of magnesium compared to other network-modifying cations.

In this study, comprehensive structural characterisation using multinuclear magic-angle spinning (MAS) and multiple quantum magic-angle spinning (MQMAS) NMR (^{27}Al, ^{11}B, ^{29}Si, ^{23}Na, ^{17}O, and ^{25}Mg) of seven glasses (with three to five oxides) was performed to clearly identify the effect of magnesium on the glass structure. Glasses enriched in ^{17}O and ^{25}Mg were also synthesised. Heteronuclear ^{11}B–^{23}Na rotational-echo double-resonance (REDOR) experiments were conducted to investigate the impact of magnesium on the spatial proximity of sodium and boron. Additionally, Raman spectroscopy was performed on all the glasses.

Most glasses in this study had constant Si/Al and Si/B ratios (close to the industrial composition of AVM V4[17,18]) with a varying Mg/Na content, except when the Mg content was found experimentally to be too high to yield a homogeneous glass. In this case, Si/Al and Si/B were decreased by 30%. A simple three-oxide (SiO_2, Na_2O, MgO) glass was prepared to confirm the specific contribution of Si–O–Mg to the ^{17}O MAS NMR spectra owing to the strong overlap of Si–O–Al, Si–O–Na and Si–O–Mg sites[34]. In addition, a glass with magnesium substituted for calcium was also examined for comparison.

2 | MATERIALS AND METHODS

2.1 | Glass synthesis and composition analysis

Twenty-four glasses, divided into four series, were synthesised using different melt-quench methods depending on their isotopic enrichment in ^{11}B, ^{17}O and ^{25}Mg. The four series are indexed as Nat (for natural/no enrichment), ^{11}B, ^{17}O, and ^{25}Mg, corresponding to their respective isotopic enrichment. ^{17}O glasses were prepared using a sol–gel process. The detailed

syntheses processes are provided for each series in the following sections. ^{11}B-enriched samples were prepared for neutron analysis, which will be reported elsewhere.

Because we focused on the impact of magnesium on the structure of the studied aluminoborosilicate glasses, the Si/Al and Si/B ratios were maintained constant when possible to synthesise a homogeneous structure (crystallisation was observed in glasses with a high magnesium content). In four glasses (N26M0, N19M8, N13M13, and N8M19), magnesium **oxide** was progressively substituted for sodium **oxide**, as shown in Table 1. N and M represent the nominal rounded concentration (mol%) of Na_2O and MgO, respectively. The amounts of aluminium and boron had to be increased in the sodium-free composition (N0M12) to obtain a homogeneous glass. Magnesium was fully substituted for calcium in the N19C8 glass. A simple reference ternary glass A0B0 (SiO_2–Na_2O–MgO) was also prepared for ^{17}O NMR spectroscopy. The composition of the glasses was analysed by inductively coupled plasma optical emission spectroscopy (ICP-OES) after **acid dissolution** (HCl + HNO_3 + HF). Additionally, some glasses were analysed using an electron probe micro-analyser at the Camparis Centre, which ensured the homogeneity of the glasses at the micrometre scale. Slight variation in composition between the series did not change the observed tendencies, as shown in Figure S1 and S2 in Supplementary Information. It can be seen that only one glass (N13M13) displayed more variation in boron coordination.**The lower fraction of B[IV] in the ^{17}O-enriched and ^{25}Mg-enriched samples can be explained by a relative higher MgO content and lower Na_2O content compared to the non-enriched glass. Indeed, as stated earlier in the manuscript, boron and sodium evaporation was more difficult to control due to the high temperature and low glass quantities. For the sake of simplicity, the discussion is based on the nominal composition, from which most of the glasses are close to.** Transmission electron microscopy (TEM) observations were also performed to ensure the absence of nanometre-scale crystallisation.

Nat and ^{11}B-enriched glasses

The seven glasses were synthesised from analytical-grade oxide **and carbonate** powders using a classical melt-quench protocol, **aiming for 180 g samples**. The powders were mixed with a Turbula® T2F to ensure homogeneity and poured into a Pt/Rh crucible, which was then placed in a Pyrox® RKA23 electric furnace equipped with a Eurotherm® 2416 regulator. Each increase in temperature occured at a rate of 300 °C.h^{-1}, while decarbonation dwell was performed at 850 °C for 1 h. The target temperature was then achieved and maintained for 3 h before quenching on a fall plate. The glasses were then crushed, and a second fusion was performed to ensure better homogeneity. These batches were then annealed (except for two impacted by crystallisation issues, namely N8M19 and N0M12) for 1.5 h in a graphite crucible at a target temperature of T_g + 20 °C, determined with a SETARAM SETSYS TMA S60/58507 operating in differential scanning calorimetry (DSC) mode under an argon atmosphere. Each temperature is given in Table 1 with the nominal compositions.

The ^{11}B enriched glasses were synthesised following the same protocol except for the boron precursor, which was replaced to achieve 99.62% enrichment **(Euriso-top**, **aiming for 20 g samples** . These glasses were prepared for a forthcoming neutron diffraction study.

^{17}O-enriched glasses

To ensure enrichment of the entire network, seven ^{17}O-enriched glasses were synthesised using a sol–gel process. This was made possible through the use of alcoxide precursors and hydrolysis reactions following Equations 1 and 2, with M and M' cations and R and R' organic groups[29].

$$M(O-R)_n + H_2^{17}O \rightarrow M(O-R)_{n-1} - {}^{17}OH + R-OH \quad (1)$$

$$M(O-R)_{n-1} - {}^{17}OH + M'(O-R) - {}^{17}OH \rightarrow (O-R)_{n-1}M - {}^{17}O - M'(O-R)_{n-1} + H_2^{17}O \quad (2)$$

The precursors were mixed with anhydrous absolute ethanol, and then with a stoichiometric amount of 90%-enriched $H_2^{17}O$ **(Cortecnet)**. After four–six weeks (to ensure full hydrolysis), the gels were dried, mixed, poured into a Pt crucible, and left overnight under argon flux in a Nabertherm® P310 electric furnace. Equivalent non-enriched glasses for composition analysis were synthesised simultaneously under the same conditions. A dehydration dwell was performed at 160 °C for 0.5 h with the temperature increasing at 300 °C.h^{-1}. Once at the target temperature T (1060 °C < T < 1400 °C), the mixture was fused for 25 min and then quenched. Because of the small glass quantities (**200 mg**), the target temperatures were reduced compared to those of the Nat glasses to minimise boron and sodium evaporation.**However, considering the small glass samples, this evaporation is more difficult to control.**

^{25}Mg-enriched glasses

All glasses were synthesised by mixing analytical-grade oxide **and carbonate** powders with 99.2% enriched ^{25}MgO **(Cortecnet** following the same route as the ^{17}O-enriched glasses except for the dwell, which was performed at 850 °C. The target temperature remained the same, i.e. 1060 °C < T < 1400 °C, **and the targeted sample mass was 300 mg**.

Glass ID	Chemical composition (mol%)						T_g (°C)	ρ
	SiO_2	B_2O_3	Al_2O_3	Na_2O	MgO	CaO		
N26M0	51.3	14.9	7.7	26.1	-	-	523	2.505
N19M8	51.2	14.9	7.7	18.7	7.5	-	573	2.45
N13M13	51.2	14.9	7.7	13.1	13.1	-	594	2.421
N8M19	51.2	14.9	7.7	7.5	18.7	-	642	2.412
N0M12	51.3	24.2	12.4	-	12.1	-	703	2.31
N19C8	51.2	14.9	7.7	18.7	-	7.5	573	2.511
A0B0	66.1	-	-	24.2	9.7	-	495	2.486

TABLE 1 Nominal targeted composition of the studied glasses, expressed in molar percent of oxide, alongside associated glass transition temperature (T_g) and measured density (ρ). The analysed composition averaged over all series fell within a standard deviation of ±2% between the series, ensuring valid comparisons. The standard deviation of the N0M12 glass reached 6% because of boron evaporation during synthesis caused by the high temperature and low mass of glass.

Sample preparation

Glass powder was obtained through grinding, sieving, and ultrasonic cleaning in both acetone and ethanol. Grinding was performed using a Retsch® MM400 with tungsten carbide balls. 20–40 µm, 63–100 µm and 100–125 µm powder fractions were selected for different experiments. The powders needed for TEM were obtained through sedimentation following Stokes' law. Square-shaped monoliths were cut and polished to achieve a surface roughness of a few nanometres.

2.2 | Structural characterisation

Nuclear Magnetic Resonance (NMR)

^{11}B, ^{23}Na, ^{27}Al, ^{29}Si, and ^{17}O MAS NMR spectra were collected on an Avance II 500WB Bruker spectrometer operating at a magnetic field of 11.72 T using a Bruker WVT CPMAS 4 mm probe (with a MAS stator free of boron oxide to avoid a strong ^{11}B signal) at a spinning frequency of 12.5 or 14 kHz. For ^{11}B, ^{23}Na, and ^{27}Al, MAS NMR spectra were acquired using a single short pulse ($\approx \pi/12$) to ensure the quantitativeness of the spectra, (because of the non homogeneous excitation of resonance of quadrupolar nuclei for long pulse) with recycle delays of 2 s, 1 s, and 1 s, respectively. ^{29}Si and ^{17}O MAS NMR spectra were acquired using a Hahn echo pulse sequence, 90°–τ_E–180°–τ_E–acquisition, with a rotor-synchronised echo delay (τ_E) of one period of rotation (for ^{17}O, soft pulses selective on the central transition were used). MQMAS experiments were performed with a Z-filter pulse sequence for ^{27}Al[59], a shifted-echo pulse sequence for ^{17}O (with an echo delay of 2 ms)[60], and a RIACT-II pulse sequence for ^{11}B and ^{23}Na[28]. For the ^{11}B–^{23}Na REDOR experiments, selective 90° and 180° pulses (at frequencies of 10 to 20 kHz and 180° pulse durations of 8 to 10 µs) were applied on the central transition (1/2↔1/2)[61].

^{25}Mg NMR data were collected on an Avance III 750 WB Bruker spectrometer operating at a magnetic field of 17.6 T using a low-gamma 4 mm CPMAS Bruker Probe at a spinning frequency of 12.5 kHz. A Hahn spin–echo pulse sequence (with selective soft pulses on the central transition, 90° ≈ 10 µs) was used with a rotor-synchronised echo delay of one rotation period and recycle delay of 0.5 s. Typically, 32768 scans were accumulated for each spectrum.

The ^{11}B, ^{23}Na, ^{27}Al, ^{29}Si, ^{17}O, and ^{25}Mg chemical shifts were referenced to external samples of a 1M boric acid solution (19.6 ppm), a 1M $AlCl_3$ aqueous solution (0 ppm), a 1M NaCl aqueous solution (0 ppm), solid tetrakistrimethylsilane (TKS) (for which the highest intensity peak is situated at 9.9 ppm from that of tetramethylsilane, TMS), ^{17}O-enriched water (0 ppm), and a 1M $MgCl_2$ aqueous solution (0 ppm).

All NMR data were processed and fitted using a custom-built code (T. Charpentier) that implements specific lineshapes for amorphous materials and accounts for the distribution of NMR parameters, as detailed in previous studies[28,29,62–64]. **In few words, the principles of our approach is to use a distribution of the NMR parameters, namely the isotropic chemical shift δ_{iso} and the quadrupolar parameters C_Q and η_Q, induced by the structural disorder inherent to the vitreous state. In a simple case such as vitreous silica,**

such NMR parameter distribution could be mapped into a distribution of geometrical parameters such as the Si–O and Si–O–Si distance[65,66]. The choice of the models were based on previous works on various compositions, ranging from simple binary sodium silicate[67] and borosilicate[68] to more complex borosilicate[28], aluminoborosilicate[57] and aluminosilicate glasses[26]. With this description of the NMR lineshapes, the NMR parameter values which are reported are therefore the mean value (and standard deviations values, i.e. the width) of the distribution (see Supplementary Information).

Raman Spectroscopy

Raman spectra were recorded using a custom-assembled system[69] comprising a Horiba iHR320 spectrometer with 1800 g.mm^{-1} gratings powered by a blue 'Sapphire SF' 488 nm laser. Short laser wavelengths are favourable for recording backscattered signals because of the increased Rayleigh scattering. The laser was focused 10 mm below the surface of the optically polished samples, allowing quantitative evaluation of the intensity. The laser excitation was rejected using a volume Bragg grating. Data were collected from 20 to 1535 cm^{-1}. The spectral window was chosen as a compromise to observe both the maximum of the boson peak and the majority of the B–O stretching modes. For the glasses presenting relatively weak Raman activity, six accumulations of 30 min were obtained in the exact same condition and position in parallel VV and perpendicular VH polarisations to be able to extract the polarisation coefficient with high precision. The spectra were corrected from the air contribution that was observed in the low-frequency region[70]. For samples showing no luminescence, no further correction or baseline was needed, and they were normalised to the total area. Brillouin spectra were recorded using a JRS TFP 2 HC tandem multipass Fabry–Perot interferometer.

3 | RESULTS

3.1 | Solid-state NMR

3.1.1 | ^{29}Si MAS NMR

For **binary alkali silicate glasses**, ^{29}Si MAS NMR provides insights into the polymerisation of the glass network through the determination of the Q_n populations[33]. However, in more complex glasses, the isotropic chemical shift is also sensitive to second-neighbour atoms (their nature and amount), which makes interpreting the signal more difficult. **At constant polymerisation degree, i.e. for a given Q_n unit,** network formers (such as Al and Zr)[28,55] tend to shift the signal to higher values, while modifiers shift the signal towards lower (i.e. more negative) values[71,72]. A broadening of the line is indicative of a more distributed silicon environment, resulting from a larger Q_n distribution or an increase in the number of Si–O–X (X = B, Al) sites. For example, overlapping of Q_3 with Si as the second neighbours and Q_4 with Al as a second neighbour has been reported in the past[73]. Generally, a shift towards a lower chemical shift value is indicative of a more polymerised network with higher Q_n species. Figure 1 shows the obtained ^{29}Si MAS NMR spectra. There was a clear decrease in the NMR shift with increasing magnesium content, as well as a broadening of the spectrum. The N8M19 glass, which had the highest magnesium content, displayed the broadest line, as did the N0M12 glass. Watts et al.[21] suggested that in bioactive glasses, this type of broadening could also result from the formation of tetrahedral magnesium inside the silicate network. When substituting calcium with magnesium (i.e. comparing N19C8 with N19M8), the line became broader and shifted to a slightly lower value, which could suggest a higher degree of polymerisation. The clear shift in the spectra to lower frequencies is reflective of Q_4 units connected to silicate units (in vitreous silica, the ^{29}Si MAS NMR spectrum is centred at approximately -110 ppm). These variations suggest the formation of a sub-network enriched in silica with increasing magnesium content. In contrast, for a low magnesium content (for example N26M0), the NMR shifts (Q_2 and Q_3) suggest a relatively depolymerised glass network.

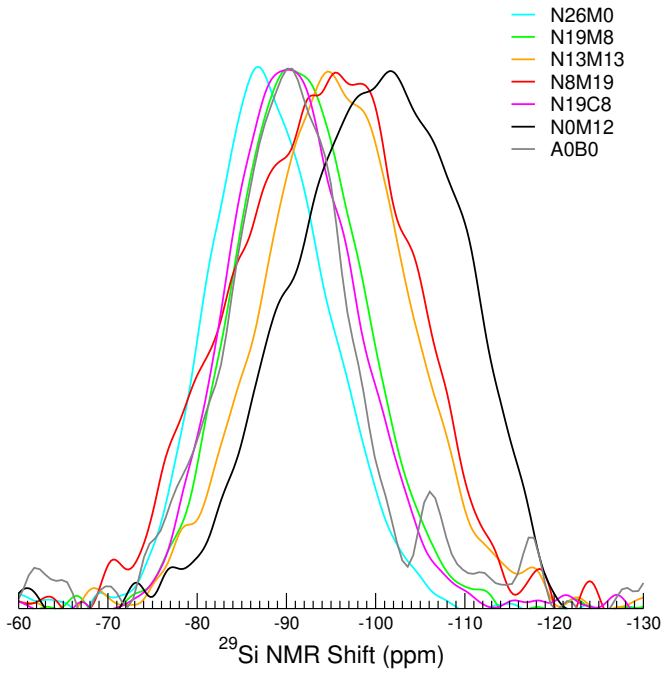

FIGURE 1 (Colour online) ^{29}Si MAS spectra for glasses in the Nat series, normalised to the maximum peak height.

3.1.2 | ^{27}Al MAS and MQMAS NMR

Figure 2 (a) shows the MAS NMR spectra obtained for the six aluminium-containing glasses in the Nat series. Except for the N0M12 glass, aluminium was predominantly found in tetrahedral units (Al[IV]). Increasing the magnesium content at the expense of sodium content (i.e. from N26M0 to N8M19) induced a slight shift in the NMR shift values as well as a slight broadening of the lines. This was most probably due to an increased distortion of the Al environment, which can be explained by the presence of Mg in the vicinity instead of Na[10]. Calculation of the full width at half maximum (FWHM) of the spectra reveals that when comparing Ca and Mg in the N19C8 and N19M8 glasses, respectively, N19C8 displays a slightly higher value. However, this might be due to small variations in the composition. For the specific case of N0M12 (no sodium), the line broadened and shifted substantially (as a result of the increase in the quadrupolar interactions, see below), and higher coordination states (Al[V] and Al[VI]) appeared. These environments were observed at approximately 30 and 3 ppm, respectively, which are typical values of such coordination[10,32,38,56]. The latter two were more visible in the MQMAS spectra, as shown in Figure 2 (c). Analysis of the MQMAS and MAS spectra yielded the population of each AlO_x species as follows: 78% Al[IV], 16% Al[V] and 6% Al[VI]. Variations in the NMR parameters are given in Table S1 and are displayed in Figure S2 in the Supplementary Information. The significant increase in the quadrupolar coupling constant for Al[IV] is clearly indicative of the impact of charge compensation by Mg cations on the local electric field gradient (EFG). Comparison with the other glass compositions suggests that Al[IV] is predominantly charge compensated by Na cations. The difference between N19M8 and N19C8 might be indicative of larger mixed charge compensation in N19C8: both Na^+ and, to a lesser extent, Ca^{2+} are in the vicinity of Al[IV], whereas in N19M8, it appears to be more difficult for Mg to contribute to the charge compensation shell.

3.1.3 | ^{11}B MAS NMR

MQMAS spectra of all the glasses are displayed in Figure 3, from which the MAS spectra and isotropic projection are extracted. NMR parameters are given in the Supplementary Information in Table S1.The B[III] and B[IV] peaks were well resolved in the ^{11}B MAS spectra, as shown in Figure 4 (a)–(b). Tetrahedral B[IV] units were characterised by a narrow peak (because of a small quadrupolar coupling constant) at approximately 0 ppm, whereas the broad shape of the planar triangular B[III] unit peak, centred around 10 ppm, is reflective of a large quadrupolar coupling constant, typically 2.4–27 MHz for B[III] units in borosilicate glasses. To quantify each unit population, it is generally found that at least two sites are

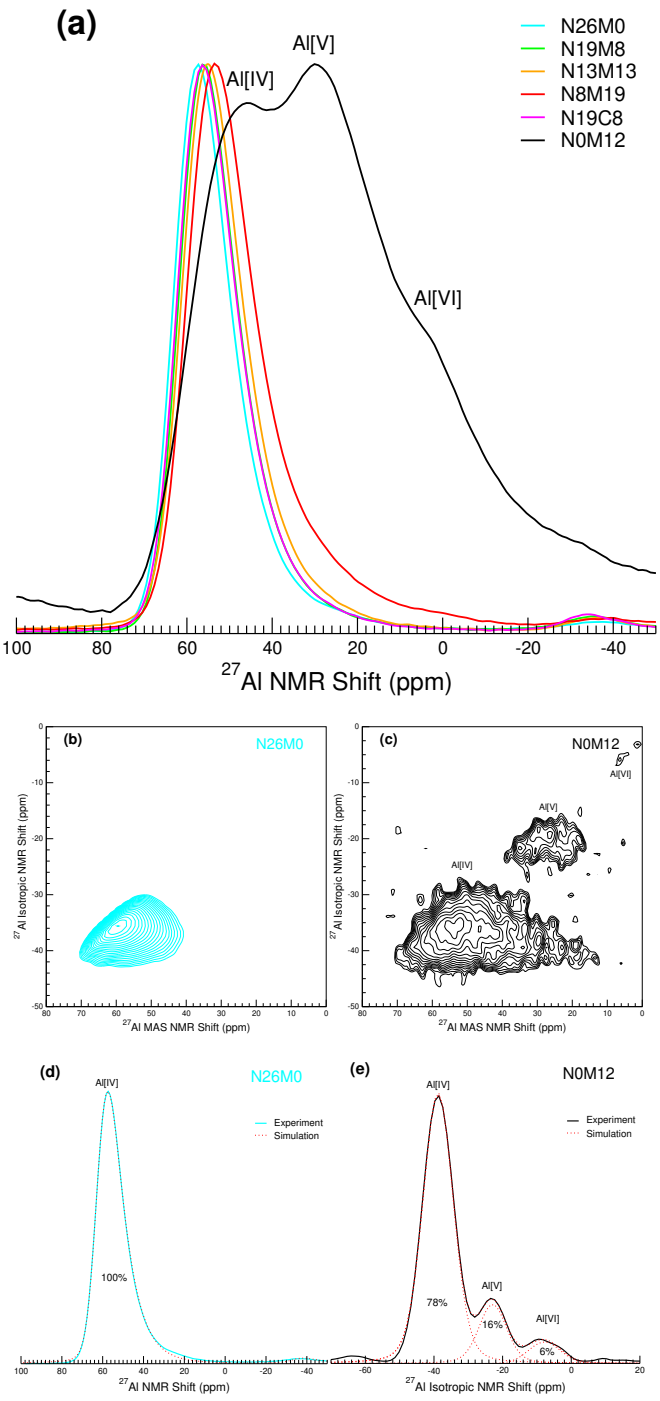

FIGURE 2 (Colour online) **(a)** ^{27}Al MAS spectra for all glasses in the Nat series, normalised to the maximum peak height. **(b)** ^{27}Al MQMAS spectra of N26M0, fully tetracoordinated, and **(c)** N0M12, for which penta- and hexacoordinated aluminium are visible. Comparison between experimental and simulated **(d)** NMR MAS spectra of N26M0 and **(e)** isotropic NMR shift of N0M12 for quantification purposes (±2%).

necessary for each coordination state. The isotropic projections of the MQMAS spectra shown in Figure 4 (c)–(d) highlight the two components for B[III] units (generally referred to as ring and non-rings units[74]) that are dependent on their connectivity to the silicate network (ring species are bonded to boron atoms). For B[IV], the asymmetric shape of the peak is also evident. A more detailed investigation of the MQMAS B[IV] peak (as well as its counterparts in the MAS spectrum) can be found elsewhere[28,75,76]. Similar to B[III], the two components can be interpreted in terms of connectivity with the silicate network (i.e. B[IV] connected to 3 or 4 SiO_2 units): an increase of Si connectivity leads to more negative isotropic chemical shifts[28,74,76].

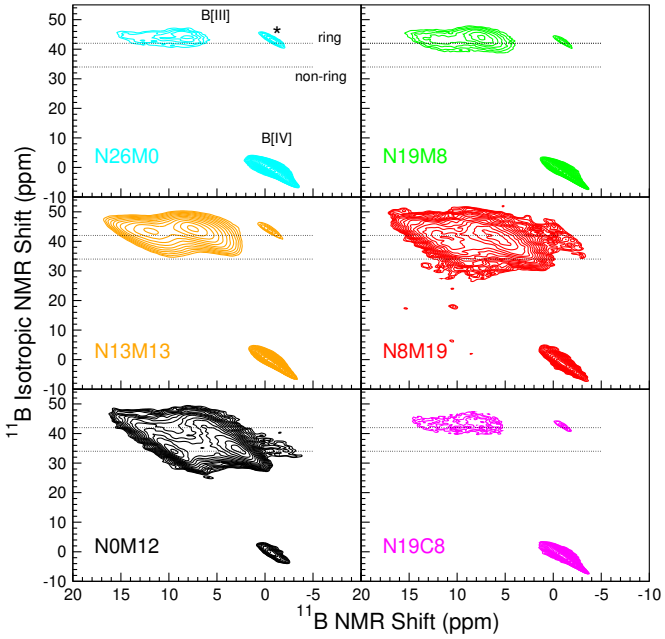

FIGURE 3 (Colour online) ^{11}B MQMAS spectra obtained from ^{11}B-enriched glasses, with the exception of N13M13 (for which the spectrum was acquired from the Nat series). Asterisks denote rotational band position for all spectra.

As shown in Figure 4 (a), progressively increasing the magnesium content at the expense of sodium resulted in an increase in B[III]. The N0M12 glass displayed the lowest B[IV] content of all the glasses, with only 2%. This increase in B[III] was also observed when substituting **magnesium for calcium** in the N19C8 and N19M8 glasses (from 54% to 63%, respectively), as shown in Figure 4 (b). Additionally, increasing the magnesium content along the series resulted in a higher contribution of B[III], associated in the literature to both non-ring and ring units, as well as when calcium was substituted by magnesium, as seen in Figure 4 (c)–(d). It appears that both sets of ^{11}B NMR data from the high-magnesium glasses show some similarities with previous experiments on SBN (SiO_2–B_2O_3–Na_2O) glasses in the immiscibility domain[77] and Pyrex glass[78], with a high B[III] ring component. These experiments suggest that magnesium could impact the glass network in a similar manner, resulting in the formation of a demixed silica/boron network at the nanoscale. When applying the Yun, Dell and Bray model, accounting for the preferential compensation of Al[IV] by sodium atoms, and considering Mg as a network modifier, modelling the %B[IV] from the glass composition shows that high magnesium glasses largely deviate from the predicted behaviour (inset in Figure 4 (a)). This indicates that the specific role of magnesium remains unclear.

3.1.4 | ^{23}Na MAS NMR

As shown in Figure 5, the ^{23}Na MAS peak moved to more negative NMR shifts with a slightly decreasing width as the magnesium content increased. The latter effect is reflective of a decrease in the quadrupolar coupling constant. The decrease in the chemical shift is indicative of a change in the role of sodium in the glass structure, from a network modifier surrounded by NBOs to a charge compensator[37]. When substituting calcium with magnesium, both effects occurred, which is consistent with the poorer charge-compensating capabilities of magnesium compared to calcium (as noticed for Al[IV] and B[IV]). The fraction of charge-compensating sodium was calculated for each glass, accounting for the B[IV] and Al[IV] fractions **i.e. considering that sodium compensated for aluminium first, then tetrahedral boron units (the remaining sodium generating NBOs) and performing the ratio of these charge-compensated units over the total number of sodium**. The results are consistent with the observed shift, ranging from 62% for N26M0 and increasing progressively to reach 100% charge-compensating sodium for N8M19. A representative MQMAS experiment is shown in Figure 5 (b): a single peak is confirmed. Variations in the NMR parameters extracted from MAS NMR are given in Table S1 and Figure S4 in the Supplementary Information. A clear increase in the isotropic chemical shift is observed, correlated to an increase in the quadrupolar coupling constant.

3.1.5 | ^{11}B{^{23}Na} REDOR

^{11}B{^{23}Na} REDOR experiments were performed to study the variation in the sodium–boron spatial proximities with the glass composition. The results are shown in Figure 6. A weaker signal indicates that there were fewer sodium atoms in the vicinity of the boron atoms. The initial slope (from 0 to 2–3 ms) reflects dipolar interactions, while the maximum value is representative of the total number of interacting atoms. The N26M0 signal was stronger with a maximum value of ≈0.9 (with a theoretical maximum of 1), indicating that 90%

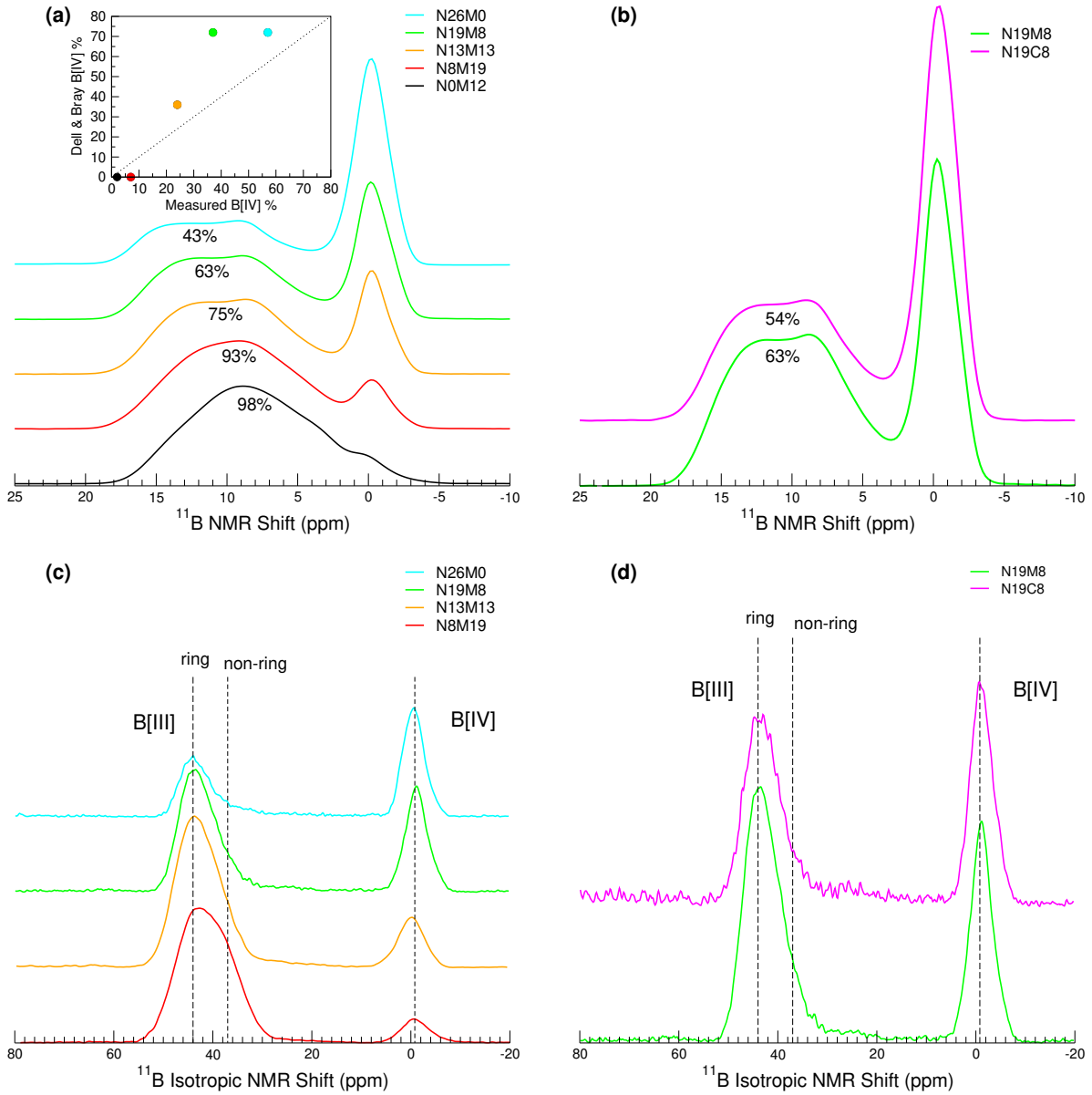

FIGURE 4 (Colour online) Experimental ^{11}B MAS spectra **(a)** of magnesium-containing glasses in the Nat series with calculated B[III] percentages (inset displays the Yun, Dell, and Bray model B[IV] calculation as a function of measured B[IV]), and **(b)** comparison between the impact of Ca and Mg on boron coordination with associated isotropic projects of ^{11}B MQMAS spectra with ring and non-ring contribution for glasses **(c)** with increasing magnesium content and **(d)** comparison between Ca and Mg in glasses. Uncertainties are given at $\pm 1\%$.

of the boron atoms had sodium atoms in their close vicinity. Taking this signal as a reference, it can be observed that the REDOR signals of N19C8 and N19M8 were very close, suggesting a similar sodium environment around the boron atoms. As expected, the signal decreased with increasing magnesium content. First, this decrease had a clear origin in the decrease in the B[IV] unit population in favour of the B[III] ring species: the latter are less likely to require sodium cations in their surroundings (no B-NBO was detected in ^{17}O NMR, see below). As a second origin, some magnesium cations could mix with sodium near NBOs[34], most probably in a boron environment. Unfortunately, this hypothesis could not be assessed with experiments such as ^{11}B{^{25}Mg} REDOR experiments (which would have required non-standard NMR equipment). However, the ^{17}O NMR data shown below do not support this

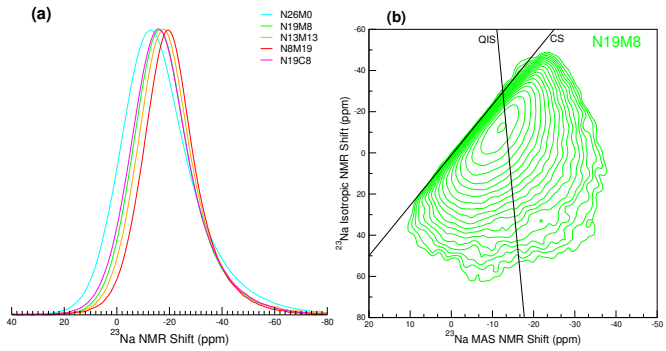

FIGURE 5 (Colour online) **(a)** ^{23}Na MAS spectra for all the relevant glasses in the Nat series, normalised to the maximum peak height and **(b)** associated MQMAS spectrum of the N19M8 glass.

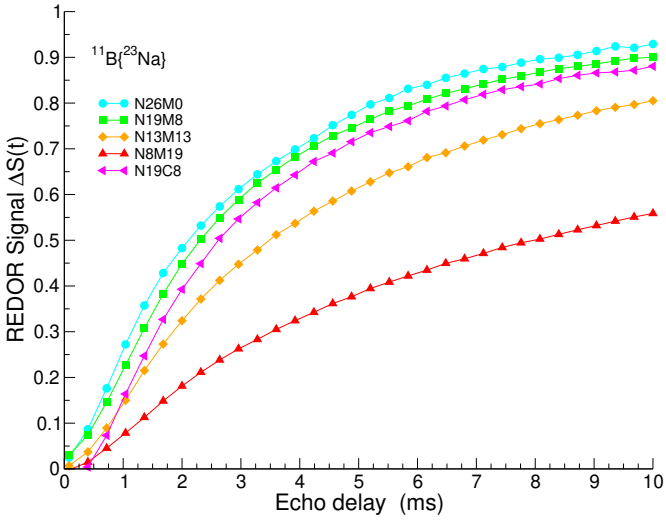

FIGURE 6 (Colour online) ^{11}B{^{23}Na} REDOR curves for the relevant glasses in the ^{11}B series.

second mechanism. Finally, it is known that sodium preferentially compensates for aluminium at the expense of boron[79,80], which is more noticeable as the sodium content decreases.

3.1.6 | ^{17}O MAS NMR

Because of the poor resolution of the ^{17}O MAS spectra (displayed in the Supplementary Information in Figure S5), triple-quantum MQMAS experiments were performed and are displayed in Figure 7. The resolution gained in the MQMAS experiments allowed for an in-depth description of the network structure. Contributions from different sites can be identified based on previously published work on borosilicate glasses[29,43,81], simpler glasses (such as sodium-aluminosilicates[31] and magnesium-aluminosilicates[32]), and both in different proportions[34].

For all studied compositions, Si–O–Al, Si–O–Na, and Si–O–Mg were hardly distinguishable, mostly because of the overlap between the resonances. The MQMAS spectra of the N19C8 and N26M0 glasses show that the Si–O–Al and Si–O–Na peaks were in the same region of isotropic NMR shifts (from –20 to –30 ppm). However, the difference in their respective quadrupolar coupling constants (3–4 MHz and 2 MHz for Si–O–Al and Si–O–Na, respectively), resulted in substancial differences in their widths along the MAS NMR shift dimension, allowing both to be visually distinguished in the N26M0 and N19C8 systems: Si–O–Na yielded a sharper peak than that of Si–O–Al. In the case of N19C8, Na–Ca mixing regions were found, as previously reported for other borosilicate glasses[29,82]. The latter was absent from all other glasses, most probably because of the strong overlap between the Si–O–Na and Si–O–Mg peaks (see A0B0). Consequently, quantitative analysis of these three peaks could not be performed using the present data. However, the similarity of the Si–O–Mg and Si–O–Al peak features (see N0M12) clearly suggests an intermediate role for Mg. For all glass compositions with Na_2O, Si–O–Na was present, suggesting the presence of NBO sites.

Regarding the borosilicate network, the isotropic projections showed that the Si–O–Si contribution (which was present for all glass compositions) shifted towards higher values with increasing magnesium content relative to the reference value of amorphous silica (–38 ppm). The intensity of the B–O–B contribution, as seen around –50 ppm, increased with the same trend, confirming the increase in ringed boron; in contrast, the Si–O–B intensity decreased. These variations are consistent with the previous suggestion that Si/B phase separation at the nanoscale was induced by the magnesium.

In addition, the percentage of NBOs, which are summarised in Table 2, can be calculated from the glass composition using Equation 3, with values given in molar atomic percent.

$$\%NBO = 100\times \frac{2\times([Na_2O]+[MgO]-[Al_2O_3]-[(B[IV])B_2O_3])}{2\times[SiO_2]+[Na_2O]+[MgO]+3\times([Al_2O_3]+[B_2O_3])} \quad (3)$$

Here, considering that Al[V] is only present in one glass in minor quantities, the assumption was made that all aluminium units are coordinated by BOs. It can be seen that the NBO percentage increased with increasing magnesium content in the series, with only slight differences when calcium was substituted by magnesium.

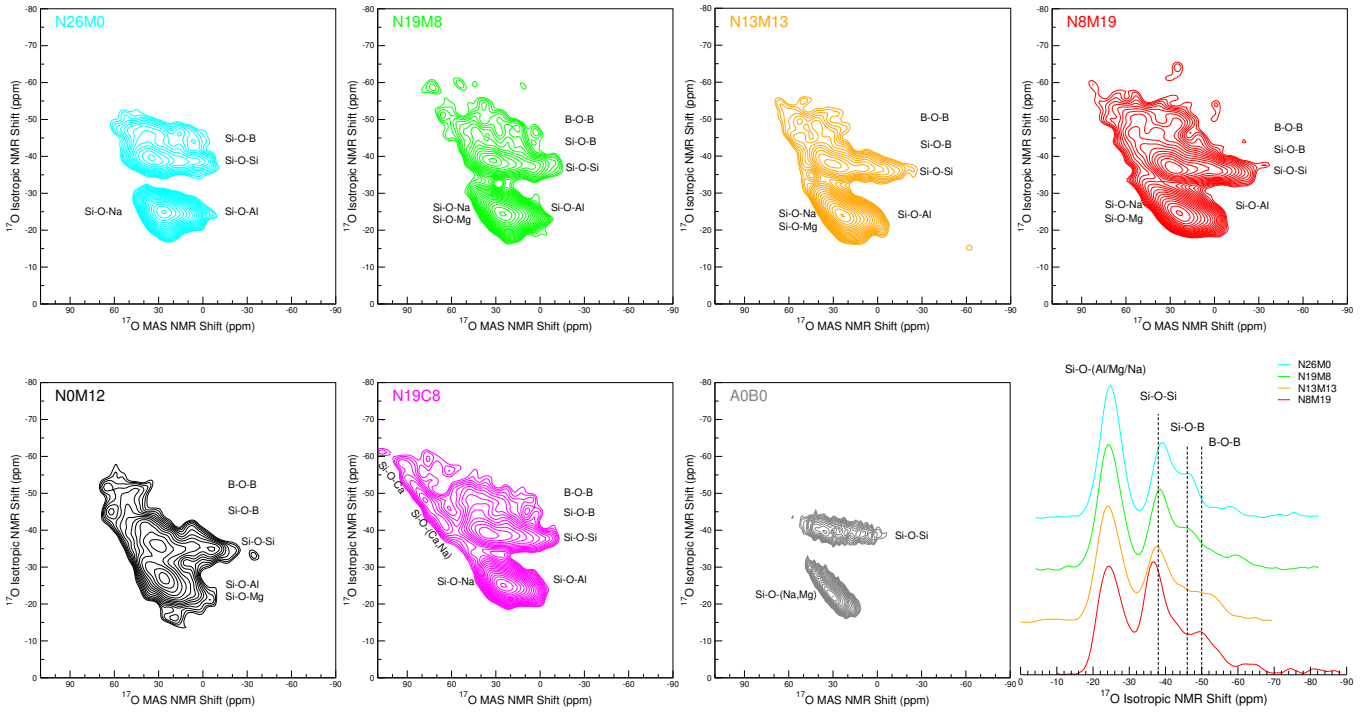

FIGURE 7 (Colour online) ^{17}O MQMAS spectra of all the studied glasses alongside ^{17}O isotropic projections of the four glasses with increasing magnesium content.

	N26M0	N19M8	N13M13	N8M19	N0M12	N19C8	A0B0
B[IV]$_{NMR}$ (%)	57	37	24	7	2	46	-
Al[IV]$_{NMR}$ (%)	100	100	100	100	78	100	-
NBO (%)	10	13	15	18	5	12	41

TABLE 2 B[IV] and Al[IV] percentages evaluated from NMR measurements with calculated total NBO% for all the glasses, following Equation 3 with compositions from Table 1.

3.1.7 | ^{25}Mg MAS NMR

Figure 8(a) shows the MAS NMR spectra obtained at a very high field (17.6 T) for the five magnesium-containing glasses. A similar strong spinning-sideband pattern was observed for all compositions. The latter suggests a high quadrupolar coupling constant that can be efficiently averaged out by the high magnetic fields and the moderate spinning frequency used (12.5 kHz). Note that for the A0B0 glass, the spinning sidebands were weaker, reflecting the more symmetrical MgO_x sites in this simple glass. The centrebands are shown in the inset of Figure 8. The observed lineshapes were close to those of ^{27}Al. A clear variation in the peak maximum was observed: it decreased with decreasing sodium content. This corroborates that the MgO_x units were less distorted in the A0B0 glass. NMR parameters were extracted by fitting the data using the same lineshapes employed for the ^{27}Al NMR spectra: a gaussian isotropic model (GIM) for the distribution of the quadrupolar parameters coupled to a Gaussian distribution of the isotropic chemical shift[62]. An example of the fitted spectra is given in the Supplementary Information in Figure S6. Mean values of the quadrupolar coupling constant C_Q (ranging from 6.5 to 8.5 MHz)e and isotropic chemical shift δ_{iso} (ranging from 5 to 35 ppm) are displayed in Figure 8 (b). A decrease in C_Q was accompanied by a decrease in δ_{iso} with increasing magnesium content for the three five-oxide glasses. N0M12 displayed the lowest δ_{iso} and highest C_Q as opposed to A0B0, which showed the highest δ_{iso} and lowest C_Q. To the best of our knowledge, these are the first data reported for ^{25}Mg

in borosilicate glasses. The impact of sodium was clearly evidenced y the decrease in the mean C_Q. This supports the idea that the MgO_x coordination sphere is stabilised by Na cations (Mg–Na mixing), resulting in less distorted (first coordination) oxygen polyhedra around Mg. Regarding the variation in the isotropic chemical shift, using trends observed for other alkali-earth cations (such as calcium)[62,83], the observed variations (increase in δ_iso) could be ascribed to a decrease of the mean Mg–O distances. Considering that Mg–NBO distances are shorter than Mg–BO (bridging oxygen) distances, the observed variation between the three groups (N0M12; N8M19, N13M13,N19M8; and A0B0) is consistent with the global increase in %NBO with increasing magnesium content (see Table 2). Slight differences between the N8M19, N13M13, and N19M8 glasses might be the results of finer effects and/or slight variations in the compositions.

3.2 | Raman spectroscopy

Raman spectroscopy was performed on all the glasses, both with vertical parallel (VV) and horizontal (VH) cross-polarisation, implying that spectra were acquired with both vertical and horizontal polarisation to see the polarisation of the vibrations more precisely. Additionally, different contributions or small variations in the spectra can be highlighted by studying the polarisation ratio of the VV to VH spectra. All the VV spectra and the polarisation ratio VV/VH are displayed in Figure 9. The VH spectra are given in the Supplementary Information in Figure S7, S8 and S9. From the VV spectra, information on the different vibrational contributions and the evolution of their concentration can be deduced directly. Only the totally symmetric vibrational modes were not acting on the polarisation. Therefore the VV/VH provides a complementary information, independent of species abundance, on the local symmetry of the atoms involved in the vibration. In general the VV spectra and the VV/VH ratio were very similar, which is normal because the symmetric vibration has a higher polarisability and is responsible for the Raman scattering[84]. Nevertheless, strong differences can be observed in Figure 9. The contribution at low Raman shifts (below 200 cm^{-1}, also called boson peak) which is related to the mid-range order of the glass, appears to be insensitive to the collection conditions, with a VV/VH ratio close to 1;this is in good agreement with the disordered state of the glass at this length scale. The position of the boson peak in the VV spectra only slightly decreased from 90 to 80 cm^{-1} with the substitution of Na by Mg. Its intensity increased, and its width narrowed slightly.

The main band between 250 and 600 cm^{-1} is commonly attributed to the bending modes of T–O–T bonds, where T denotes for tetrahedra[85]. Figure 9 (a) shows that increasing the magnesium content at the expense of sodium induced both a

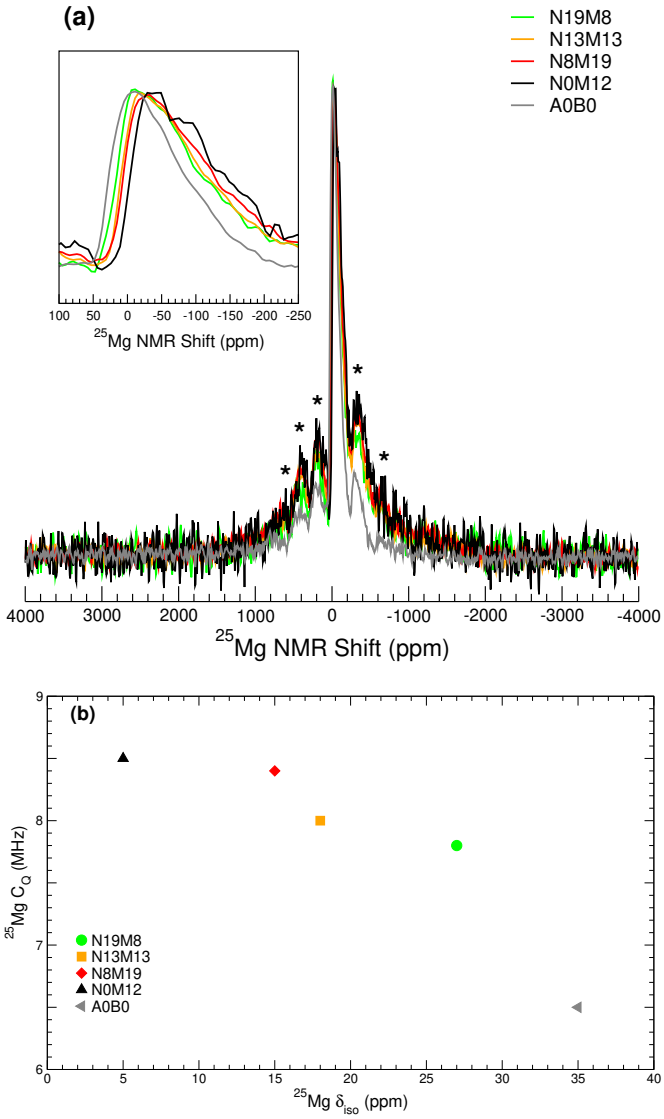

FIGURE 8 (Colour online) **(a)** Full ^{25}Mg MAS spectra, with the inset magnifying on the –250 – 100 ppm region. Asterisks are used to denote spinning sidebands. **(b)** Calculated quadrupolar coupling constant versus isotropic chemical displacement of the five ^{25}Mg-enriched glasses.

shift to lower frequencies, indicative of an opening of the Si–O–Si angle linked to a higher degree of polymerisation, and an increase in the intensity of this band at the expense of the Q_n band, between 850 and 1275 cm^{-1} [86–88]. This shift also occured to a lesser extent when calcium was substituted with magnesium, as shown in Figure 9 (b). The D2 band at 600 cm^{-1}, assigned to three-membered T rings, tended to merge with the main band with increasing Mg content. The VV/VH ratio over the full main band region remained unchanged. The second part of the Raman spectra linked with tetrahedra is the Q_n region between 850 and 1200 cm^{-1}. In this region, the band broadens in both Figure 9 (a) and (b), which indicates

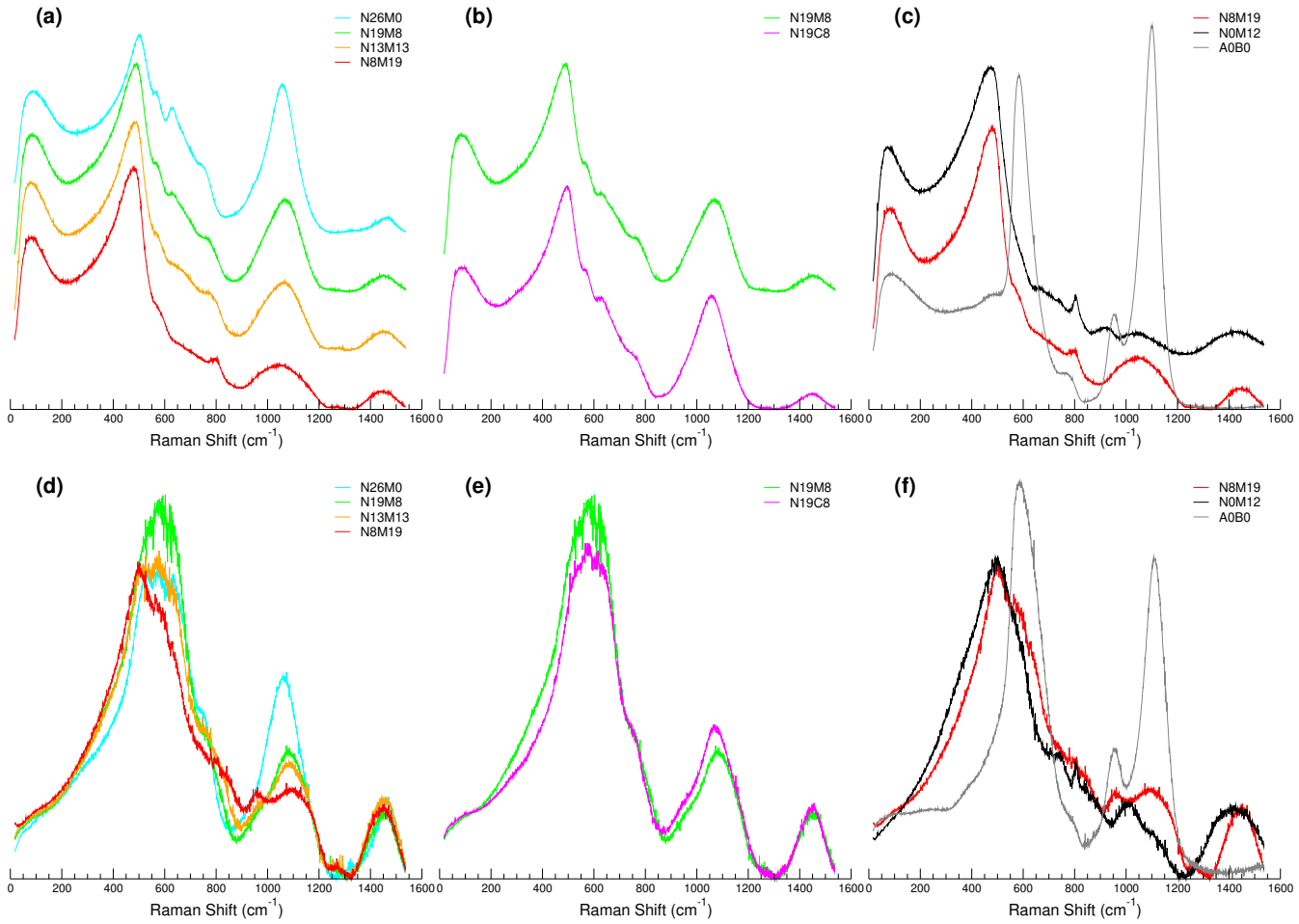

FIGURE 9 (Colour online) Peak-area-only normalised Raman spectra obtained with VV polarisation **(a)** for the glasses with increasing magnesium content, **(b)** comparison between the calcium and magnesium containing glasses and **(c)** comparison between the highest magnesium-containing glass with the two simplest glasses as reference. **(d)**, **(e)**, and **(f)** shown their respective VV/VH ratios.

a higher distribution of the environment. While compositions differs significantly among the three glasses in Figure 9 (c), it is important to note the apparent separation between Q_4 and Q_3 units (found around 1150 and 1100 cm^{-1}, respectively) to Q_2 and potentially Q_1 units (found around 955 and 890 cm^{-1}, respectively) for both N0M12 and A0B0, which were not clearly distinguishable for the N8M19 glass. The results obtained for A0B0 are consistent with those observed for similar compositions by Trcera et al.[89] and Hehlen and Neuville[90]. The ratio between the signals obtained with VV and VH polarisations, as displayed in Figure 9 (d)–(f) allows clearer visualisation of Q_2 for the N8M19 glass as well as the decrease in shift values for the N0M12, indicative of a higher presence of Q_2 compared to Q_3 in this glass. The strong decrease in VV/VH in all Q_n regions with the substitution of Na by Mg indicates that the apparent decrease in the intensity of the Q_3 in the VV spectra is associated with a strong symmetry lowering with the introduction of Mg. As shown Figure 9 (e), a similar but slightly weaker effect was observed with Ca. This symmetry loss can be attributed to the double charge of both Ca and Mg, which compensate for the NBO in a less homogeneous manner. The breathing modes of borate/borosilicate rings are typically found in the range of 550 to 850 cm^{-1} [85,91,92], in which danburite-type B_2O_7-Si_2O_7 ring contributions ascribed to 630 cm^{-1} can be isolated[85]. The latter contribution disappeared completely at high magnesium contents. Parallel vibrational contributions of pentaborate and/or boroxol units around 780–800 cm^{-1} appeared with increasing magnesium content in the glass series. It can be assumed that the disappearance of the danburite units led to the formation of pentaborate and/or boroxol units. No clear contribution of these borate units can be seen in the VV/VH ratio, suggesting that they have poor symmetry; therefore, they are bent

or deformed. Only slight variations were observed when calcium was substituted with magnesium, making a comparison between the two non-conclusive. At the end of the spectra (1300–1500 cm^{-1}), there were contributions arising from B–O stretching vibrations linked to B[III] units, consisting of different Gaussian components, 1320 cm^{-1} for loose B[III] units, 1410 cm^{-1} for B[III] units linked to B[IV], 1480 cm^{-1} for B[III] linked to B[III], and 1515 cm^{-1} for B[III] linked to boroxol units[87,93–97]. N0M12 is the only glass presenting a strong contribution at 1320 cm^{-1} in Figure 9 (f). The presence of loose B[III] units can be explained by the high quantity of B atoms. In this condition, isolated B[III] units can be hypothesised within the silica network. For all the other glasses, only the contributions at 1410 and 1480 cm^{-1} were observed. A small broadening of the low-frequency band was observed with increasing magnesium content in the series; it indicated a higher proportion of tri-coordinated boron. This is consistent with the ^{11}B NMR results. However the magnitude of this modification was significantly lower what was expected, suggesting the B units lowering their coordination preferentially vibrated within ring structures in the 800 cm^{-1} region. No broadening was observed when calcium was substituted with magnesium.

4 | DISCUSSION

4.1 | Impact of magnesium on the structure

The most salient effect of magnesium incorporation on the vitreous network is an increase in the B[III] population. In this work, the increase in magnesium was made at the expense of sodium, but this effect has also been reported with a constant sodium content[10,14] to a lesser extent. As expected, the highest B[IV] content was reached for the N26M0 glass, with a value of 57%. Based on the composition, calculations from the Yun, Dell and Bray[98–100] (YDB) model predicted a much larger value, 72% B[IV], which considers that the sodium compensating for aluminium cannot compensate for boron and based is on the target compositions given in Table 1. Among all the glasses, only N26M0 possessed excess sodium to form NBOs with up to 3.5% Na_2O available even if boron was 100% tetracoordinated. This behaviour was evident in the ^{23}Na NMR spectrum as a shift towards higher isotropic chemical shift values[37], and the appearance of a contribution at 1320 cm^{-1} in the Raman spectra.

When 7.5% sodium was substituted with calcium (N19C8), the B[IV] fraction decreases by 11%, reaching 46%. The YDB model once again gave a much higher value (71%). This significant decrease can be ascribed to the formation of Ca–Na mixing sites near NBO-rich regions in the glass, which has been previously observed[42,43] and was also visible in the ^{17}O spectrum. Such sites prevent sodium from charge-compensating tetrahedral boron, in addition to calcium, which does not compensate for boron. Another 9% decrease in the B[IV] proportion was observed when 7.5% of the calcium was substituted by magnesium in the same proportion (N19M8). This has also been seen in different compositions by Backhouse et al.[14] or Lograd et al.[12]. Quintas et al.[101,102] noticed that the cation mean field strength (MFS, see Equation 4) affects its ability to charge-compensate for boron atoms. A higher MFS induces a decrease in the charge-compensating abilities[56,58,79,103].

$$MFS = \frac{z}{r^2} \tag{4}$$

z: cation charge, r: mean distance between the cation and an oxygen.

Calculation thus gives an estimated MFS of 0.45 $Å^{-2}$ for magnesium and 0.35 $Å^{-2}$ for calcium, which could be a first explanation to the decrease in%B[IV] with increasing magnesium content. However, int the ^{17}O NMR spectra of this glass, Mg–Na mixing sites near NBOs could not be distinguished as clearly as Ca–Na mixing sites in the calcium-containing glass due to the considerable overlap of contributions arising from Si–O–Al, Si–O–Na, and Si–O–Mg, as seen in the simplest glass (A0B0). Simulations of NMR spectra using density functional theory (DFT) calculations combined with MD simulations will be performed in the future to attempt to more precisely ascribe such sites[104]. Furthermore, the substitution of calcium (and sodium) by magnesium generate a B[III] contribution arising from the boron rings. This result was more striking in the MQMAS isotropic projections, as shown in Figure 4 (c)–(d), than in the Raman spectra, even though there appeared to be a slight increase in the peak in the 780 to 800 cm^{-1} range. The ^{29}Si NMR spectra for both N19C8 and N19M8 shifted to lower values, accompanied by a slight broadening, which could be attributed to the formation of more polymerised silica domains compared to those in the glass without sodium. This result is supported by the Raman spectra, which displayed what is typically ascribed to an aperture of the Si–O–Si angle, as well as the isotropic projections of the ^{17}O glasses, which displayed variations in the Si–O–Si isotropic shift.

A further increase in magnesium content to 13.1% at the expense of sodium resulted in lower B[IV] fractions, reaching 25%, accompanied by a higher contribution of B[III] ring units. This is confirmed by the Raman spectra where a new peak emerges at 750 and 800 cm^{-1} (contribution better seen in the VV/VH ratio). The slight variation of the B[III] vibrational contribution at 1400 cm^{-1} and above could confirm the ring nature of the newly formed B[III] units. The ^{29}Si spectra displayed an even larger shift towards lower values as well as a significant broadening of the line. This indicates the progressive formation of more polymerised Q_n units but also a

larger distribution of silicon environments, which is supported by the Raman spectrum with a slight shift towards higher wavenumber. Additionally, the ^{17}O spectrum showed a slight broadening in the Si–O–Si contribution. Finally, a slight broadening occured in the ^{27}Al spectrum, which could indicate a small proportion of magnesium in the vicinity of aluminium, distorting the tetrahedra.

When sodium is available in a similar proportion to that of aluminium (e.g. N8M19), it appears that magnesium also compensates for aluminium (fully tetra-coordinated) to a greater extent than in N13M13. This results in a larger broadening of the ^{27}Al NMR spectrum, similar to what has already been observed for calcium[67]. Moreover, magnesium could participate in the compensation of a small amount of boron (7% B[IV]). REDOR ^{11}B–^{23}Na NMR experiments showed a high decrease in boron–sodium proximity, indicating that part of the boron could be compensated by magnesium. This could also be ascribed to the fact that when aluminium is compensated by magnesium in this glass, a small proportion of sodium is available to compensate for B[IV] units. This is supported by the ^{23}Na spectra obtained on for all the glasses in the series, for which the chemical shift evolved in the same manner as the change in the proportion of sodium behaving as a modifier to a full charge compensator. For this glass, the ^{29}Si NMR spectrum displayed an even larger broadening, which could indicate a separation in several Q_n units. The Raman spectra VV/VH ratio revealed two distinct bands in the Q_n region, which supports this hypothesis. A comparison between the spectra obtained in this region on this glass and those of the ternary A0B0 (similar to the NMS3 and NMS4 studied by Trcera et al.[89]) suggests that this separation could be attributed to some extent to the formation of Q_4 units, with a decrease in Q_3 and an increase in Q_2 units. Q_2- and Q_4-rich regions could thus originate from magnesium in the glass in a similar way to calcium[105]. This effect could also be intensified by a higher MFS[106], which, in some ternary glasses, also tends to generate more Q_4. It is interesting to note that when the magnesium content in the series increased, there was a significant increase in the ringed boron contribution. This could also imply the formation of a boron-rich sub-network, which is further supported by the increase in Si–O–B and B–O–B contributions observed in the ^{17}O spectra as well as the increase in intensity observed in the 750–800 cm^{-1} region in the Raman spectrum.

Finally, when no sodium was available to compensate for boron, as in the N0M12 glass, the B[IV] population dramatically decreased, reaching a value as low as 2%. This demonstrates that only a small fraction of boron can be compensated by magnesium, thus corroborating that magnesium is most probably not involved in charge compensation in the other studied glasses. Additionally, ≈78% of aluminium was compensated by magnesium in tetrahedral units while 96% compensation was possible based on the magnesium content. The roles of the higher-coordination states Al[V] and Al[VI] remain unclear. In the same way as for boron, magnesium can only partly compensate for aluminium. **Based on previous work performed by Allwardt and Stebbins on K–Mg and Ca–Mg silicates[107], our data may also suggest a preferential association of Mg to NBOs rather than BOs, resulting in the observed poor ability to act as a charge compensator. Indeed, considering the small radius and high charge of Mg^{2+} compared to Na^+, Mg^{2+} can be expected to be found mostly near concentrated negative charges, i.e. NBOs, thus less eager to associate with more diluted charge distribution, i.e. B[IV] and Al[IV].** Consequently, the ^{29}Si NMR spectra displayed a large broadening, indicative of highly distributed Q_n species, from slightly polymerised to highly polymerised units. The high boron content in this glass could partly explain this phenomenon: second-neighbour boron tends to shift ^{29}Si spectra in the same manner as a decrease in the polymerisation degree[73]. Raman spectra displayed a shift of the Q_n band towards lower units and a separate contribution at 925 cm^{-1} too low to be assigned to regular Q_2 units. This could result in the formation of a Si–O–Si-rich sub-network as well as a Si–O–B-rich sub-network. Finally, it has also been suggested that, in bioactive glasses, an increase in higher Q_n species or a shift towards lower chemical shift values with increasing magnesium content could result from the formation of tetrahedral MgO_4 entering the silicate network as an intermediate oxide[21].

4.2 | Magnesium environment in the studied glasses

Some studies suggest that magnesium can be found in both tetrahedral and octahedral forms in glasses, even if the calculation gives a mean coordination number value of approximately five[20,46]. The presence of tetrahedral magnesium indicates that it could behave similar to an intermediate cation: between a network former and modifier[12,15,21,24,108]. Watts et al.[21] suggested that this behaviour is more often seen in a highly disrupted glass. Additionally, competition with aluminium in the attraction of neighbouring oxygen by magnesium could occur because of the rather short Mg–O bond length. In pyroxene-like glasses, the coordination of magnesium remains uncertain because there were four short 2.08 Å and two long 2.5 Å bonds, thus raising the question of whether the latter two should be considered to be part of the coordination sphere[15,109] in this type of glass.

It is difficult to determine the coordination number of magnesium in glasses using NMR. Most data available on ^{25}Mg NMR were obtained in crystalline materials, with only few on silicates. The studied systems are typically less complex than

those in the present study[48], apart from very recent ones[15]. The X-ray absorption near edge structure (XANES) study performed on NMS3 and NMS4 by Trcera et al.[89], with compositions relatively close to A0B0 in the study, suggests that magnesium coordination is between five and six in this glass and that no change is observed in magnesium coordination with increasing or decreasing degree of polymerisation. The calculated δ_{iso} extracted from the ^{25}Mg NMR spectrum for this glass gives a value of 35 ppm, which falls within the range of penta-coordinated magnesium when compared to data for both glasses and crystalline materials[19,48,50,51]. When the magnesium content increase in the glass series, the value of δ_{iso} decreased. The progressive decrease in δ_{iso} implies that magnesium mean coordination progressively shifts from five to six. This is also suggested by the width of the chemical shift in all these glasses, as suggested by Shimoda et al. for several simple glasses[46], but does not exclude the presence of tetrahedral units. Conversely, the C_Q values increased with increasing magnesium content in the series. Th highest C_Q and lowest δ_{iso} values were obtained for the four-oxide N0M12 with no sodium. In this glass, magnesium should be found in the octahedral coordination. Future calculation of Mg–O bond distances (Mg–BO and Mg–NBO) and coordination numbers by classical MD as well as values extracted from neutron diffraction spectra of these glasses might allow a more precise and comprehensive analysis of their magnesium environments.

5 | CONCLUSION

Four magnesium-containing aluminoborosilicate glasses, a complementary calcium-containing glass, a sodoaluminoborosilicate glass, and a simple reference silicate glass were studied through extensive structural characterisation by multinuclear NMR analysis and Raman spectroscopy. The impact of the progressive incorporation of magnesium (at the expense of sodium) on the structure of these glasses was investigated.

The most prominent effect of magnesium is a dramatic decrease in the mean boron coordination number. This can be ascribed to the poor charge-compensating capability of magnesium of B[IV] units, which is linked to a relatively high MFS, coupled with the consumption of sodium atoms in magnesium–sodium mixing domains. In return, boron tends to reorganise and partly form boroxol rings, reducing Si/B mixing.

Similarly, magnesium appears to be less able to compensate for tetrahedral aluminium when sodium is present. When less sodium is available in the vicinity of aluminium, a progressive distortion of aluminium tetrahedra appears, yielding a higher quadrupolar coupling constant. When no sodium is available, the formation of pentahedral and octahedral units (≈25%) is observed.

These structural modifications promote an overall reorganisation of the silicon network which appears to induce the formation of a highly polymerised sub-network as well as less-polymerised mixed magnesium–sodium regions when the magnesium content increases. Finally, the mean coordination of magnesium in these glasses shift progressively from most likely five to six as the proportion of magnesium increases, but ^{25}Mg MAS NMR at a high field (17.6 T) could not resolve these coordination numbers.

ACKNOWLEDGEMENTS

This study was supported by the French Alternative Energies and Atomic Energy Commission (CEA) and Electricité de France (EDF). Financial support from the IR-RMN-THC FR 3050 CNRS for conducting the research (^{25}Mg MAS NMR) is gratefully acknowledged.

BIBLIOGRAPHY

References

[1] D. L. Morse and J. W. Evenson. Welcome to the Glass Age. International Journal of Applied Glass Science, 7(4):409–412, 2016.

[2] Bijaya B. Karki and Lars P. Stixrude. Viscosity of MgSiO3; Liquid at Earth's Mantle Conditions: Implications for an Early Magma Ocean. Science, 328(5979):740, 2010.

[3] Lars Stixrude and Bijaya Karki. Structure and Freezing of MgSiO3; Liquid in Earth's Lower Mantle. Science, 310(5746):297, 2005.

[4] J. M. Oliveira, R. N. Correia, M. H. Fernandez, and J. Rocha. Influence of the CaO/MgO ratio on the structure of phase-separated glasses: a solid state Si-29 and P-31 MAS NMR study. Journal of Non-Crystalline Solids, 265(3):221–229, 2000.

[5] T. Kokubo, H. Kushitani, C. Ohtsuki, S. Sakka, and T. Yamamuro. Chemical reaction of bioactive glass and glass-ceramics with a simulated body fluid. Journal of Materials Science: Materials in Medicine, 3(2):79–83, 1992.

[6] M. Diba, F. Tapia, A. R. Boccaccini, and L. A. Strobel. Magnesium-Containing Bioactive Glasses for Biomedical Applications. International Journal of Applied Glass Science, 3(3):221–253, 2012.

[7] D. Bellucci, E. Veronesi, M. Dominici, and V. Cannillo. A new bioactive glass with extremely high crystallization temperature and outstanding biological performance. Materials Science & Engineering C-Materials for Biological Applications, 110, 2020.

[8] John C. Mauro, Adama Tandia, K. Deenamma Vargheese, Yihong Z. Mauro, and Morten M. Smedskjaer. Accelerating the Design of Functional Glasses through Modeling. Chemistry of Materials, 28(12):4267–4277, 2016.

[9] T. K. Bechgaard, G. Scannell, L. P. Huang, R. E. Youngman, J. C. Mauro, and M. M. Smedskjaer. Structure of MgO/CaO sodium aluminosilicate glasses: Raman spectroscopy study. Journal of Non-Crystalline Solids, 470:145–151, 2017.

[10] H. Bradtmuller, T. Uesbeck, H. Eckert, T. Murata, S. Nakane, and H. Yamazaki. Structural Origins of Crack Resistance on Magnesium Aluminoborosilicate Glasses Studied by Solid-State NMR. Journal of Physical Chemistry C, 123(24):14941–14954, 2019.

[11] M. Y. Wang, M. M. Smedskjaer, J. C. Mauro, G. Sant, and M. Bauchy. Topological Origin of the Network Dilation Anomaly in Ion-Exchanged Glasses. Physical Review Applied, 8(5), 2017.

[12] Millena Lograd, Hellmut Eckert, Tetsuya Murata, Shingo Nakane, and Hiroki Yamazaki. Structure-property relations in crack-resistant alkaline-earth aluminoborosilicate glasses studied by solid state NMR. Journal of the American Ceramic Society, 2021. WOS:000610789200001.

[13] Stéphane Gin, Xavier Beaudoux, Frédéric Angéli, Christophe Jégou, and Nicole Godon. Effect of composition on the short-term and long-term dissolution rates of ten borosilicate glasses of increasing complexity from 3 to 30 oxides. Journal of Non-Crystalline Solids, 358(18):2559–2570, September 2012.

[14] D. J. Backhouse, C. L. Corkhill, N. C. Hyatt, and R. J. Hand. Investigation of the role of Mg and Ca in the structure and durability of aluminoborosilicate glass. Journal of Non-Crystalline Solids, 512:41–52, 2019.

[15] R. Guo, C. T. Brigden, S. Gin, S. W. Swanton, and I. Farnan. The effect of magnesium on the local structure and initial dissolution rate of simplified UK Magnox waste glasses. Journal of Non-Crystalline Solids, 497:82–92, 2018.

[16] M. T. Harrison. The effect of composition on short- and long-term durability of UK HLW glass. 2nd International Summer School on Nuclear Glass Wasteform: Structure, Properties and Long-Term Behavior (Sumglass 2013), 7:186–192, 2014.

[17] B. M. J. Thien, N. Godon, A. Ballestero, S. Gin, and A. Ayral. The dual effect of Mg on the long-term alteration rate of AVM nuclear waste glasses. Journal of Nuclear Materials, 427(1-3):297–310, 2012.

[18] E. Vernaz and J. Brueziere. History of Nuclear Waste Glass in France. 2nd International Summer School on Nuclear Glass Wasteform: Structure, Properties and Long-Term Behavior (Sumglass 2013), 7:3–9, 2014.

[19] P. S. Fiske and J. F. Stebbins. The Structural of Mg in Silicate Liquids - a High-Temperature Mg-25, Na-23, and Si-29 Nmr-Study. American Mineralogist, 79(9-10):848–861, 1994.

[20] Keiji Shimoda, Yasuhiro Tobu, Moriaki Hatakeyama, Takahiro Nemoto, and Koji Saito. Structural investigation of Mg local environments in silicate glasses by ultra-high field 25Mg 3QMAS NMR spectroscopy. American Mineralogist, 92(4):695–698, 2007.

[21] S. J. Watts, R. G. Hill, M. D. O'Donnell, and R. V. Law. Influence of magnesia on the structure and properties of bioactive glasses. Journal of Non-Crystalline Solids, 356(9):517–524, 2010.

[22] Marie Guignard and Laurent Cormier. Environments of Mg and Al in MgO–Al2O3–SiO2 glasses: A study coupling neutron and X-ray diffraction and Reverse Monte Carlo modeling. Chemical Geology, 256(3):111–118, November 2008.

[23] L. Cormier and G. J. Cuello. Structural investigation of glasses along the MgSiO3-CaSiO3 join: Diffraction studies. Geochimica Et Cosmochimica Acta, 122:498–510, 2013.

[24] A. Pedone, G. Malavasi, M. C. Menziani, U. Segre, and A. N. Cormack. Role of magnesium in soda-lime glasses: insight into structural, transport, and mechanical properties through computer simulations. Journal of Physical Chemistry C, 112(29):11034–11041, 2008.

[25] M. C. Wilding, C. J. Benmore, J. A. Tangeman, and S. Sampath. Evidence of different structures in magnesium silicate liquids: coordination changes in forsterite-

to enstatite-composition glasses. Chemical Geology, 213(1-3):281–291, 2004.

[26] D. R. Neuville, L. Cormier, V. Montouillout, P. Florian, F. Millot, J. C. Rifflet, and D. Massiot. Structure of Mg- and Mg/Ca aluminosilicate glasses: Al-27 NMR and Raman spectroscopy investigations. American Mineralogist, 93(11-12):1721–1731, 2008.

[27] N. Trcera, S. Rossano, and M. Tarrida. Structural study of Mg-bearing sodosilicate glasses by Raman spectroscopy. Journal of Raman Spectroscopy, 42(4):765–772, 2011.

[28] F. Angeli, T. Charpentier, D. de Ligny, and C. Cailleteau. Boron Speciation in Soda-Lime Borosilicate Glasses Containing Zirconium. Journal of the American Ceramic Society, 93(9):2693–2704, 2010.

[29] F. Angeli, T. Charpentier, M. Gaillard, and P. Jollivet. Influence of zirconium on the structure of pristine and leached soda-lime borosilicate glasses: Towards a quantitative approach by O-17 MQMAS NMR. Journal of Non-Crystalline Solids, 354(31):3713–3722, 2008.

[30] S. Kroeker and J. F. Stebbins. Magnesium coordination environments in glasses and minerals: New insight from high-field magnesium-25 MAS NMR. American Mineralogist, 85(10):1459–1464, 2000.

[31] S. K. Lee and J. F. Stebbins. Effects of the degree of polymerization on the structure of sodium silicate and aluminosilicate glasses and melts: An O-17 NMR study. Geochimica Et Cosmochimica Acta, 73(4):1109–1119, 2009.

[32] S. K. Lee, H. I. Kim, E. J. Kim, K. Y. Mun, and S. Ryu. Extent of Disorder in Magnesium Aluminosilicate Glasses: Insights from Al-27 and O-17 NMR. Journal of Physical Chemistry C, 120(1):737–749, 2016.

[33] H. Maekawa, T. Maekawa, K. Kawamura, and T. Yokokawa. The Structural Groups of Alkali Silicate-Glasses Determined from Si-29 Mas-Nmr. Journal of Non-Crystalline Solids, 127(1):53–64, 1991.

[34] S. Y. Park and S. K. Lee. Probing the structure of Fe-free model basaltic glasses: A view from a solid-state Al-27 and O-17 NMR study of Na-Mg silicate glasses, Na2O-MgO-Al2O3-SiO2 glasses, and synthetic Fe-free KLB-1 basaltic glasses. Geochimica Et Cosmochimica Acta, 238:563–579, 2018.

[35] Hellmut Eckert. Spying with spins on messy materials: 60 Years of glass structure elucidation by NMR spectroscopy. International Journal of Applied Glass Science, 9(2):167–187, 2018.

[36] Randall Youngman. NMR Spectroscopy in Glass Science: A Review of the Elements. Materials, 11(4):476, April 2018.

[37] F. Angeli, J. M. Delaye, T. Charpentier, J. C. Petit, D. Ghaleb, and P. Faucon. Influence of glass chemical composition on the Na-O bond distance: a (23)Na 3Q-MAS NMR and molecular dynamics study. Journal of Non-Crystalline Solids, 276(1-3):132–144, 2000.

[38] K. E. Kelsey, J. R. Allwardt, and J. F. Stebbins. Ca-Mg mixing in aluminosilicate glasses: An investigation using O-17 MAS and 3QMAS and Al-27 MAS NMR. Journal of Non-Crystalline Solids, 354(40-41):4644–4653, 2008.

[39] K. E. Kelsey, J. F. Stebbins, L. S. Du, J. L. Mosenfelder, P. D. Asimow, and C. A. Geiger. Cation order/disorder behavior and crystal chemistry of pyrope-grossular garnets: An O-17 3QMAS and Al-27 MAS NMR spectroscopic study. American Mineralogist, 93(1):134–143, 2008.

[40] H. I. Kim and S. K. Lee. The degree of polymerization and structural disorder in (Mg,Fe)SiO3 glasses and melts: Insights from high-resolution Si-29 and O-17 solid-state NMR. Geochimica Et Cosmochimica Acta, 250:268–291, 2019.

[41] S. K. Lee and E. J. Kim. Probing Metal-Bridging Oxygen and Configurational Disorder in Amorphous Lead Silicates: Insights from O-17 Solid-State Nuclear Magnetic Resonance. Journal of Physical Chemistry C, 119(1):748–756, 2015.

[42] S. K. Lee and J. F. Stebbins. Nature of cation mixing and ordering in Na-Ca silicate glasses and melts. Journal of Physical Chemistry B, 107(14):3141–3148, 2003.

[43] F. Angeli, T. Charpentier, E. Molieres, A. Soleilhavoup, P. Jollivet, and S. Gin. Influence of lanthanum on borosilicate glass structure: A multinuclear MAS and MQMAS NMR investigation. Journal of Non-Crystalline Solids, 376:189–198, 2013.

[44] S. Kroeker, P. S. Neuhoff, and J. F. Stebbins. Enhanced resolution and quantitation from 'ultrahigh' field NMR spectroscopy of glasses. Journal of Non-Crystalline Solids, 293:440–445, 2001.

[45] S. Sen, H. Maekawa, and G. N. Papatheodorou. Short-Range Structure of Invert Glasses along the Pseudo-Binary Join MgSiO3-Mg2SiO4: Results from Si-29 and Mg-25 MAS NMR Spectroscopy. Journal of Physical Chemistry B, 113(46):15243–15248, 2009.

[46] K. Shimoda, T. Nemoto, and K. Saito. Local structure of magnesium in silicate glasses: A Mg-25 3QMAS NMR study. Journal of Physical Chemistry B, 112(22):6747–6752, 2008.

[47] B. Zhou, A. Faucher, R. Laskowski, V. V. Terskikh, S. Kroeker, W. Sun, J. R. Lin, J. X. Mi, V. K. Michaelis, and Y. M. Pan. Ultrahigh-Field Mg-25 NMR and DFT Study of Magnesium Borate Minerals. Acs Earth and Space Chemistry, 1(6):299–309, 2017.

[48] J. C. C. Freitas and M. E. Smith. Recent Advances in Solid-State Mg-25 NMR Spectroscopy. Annual Reports on Nmr Spectroscopy, Vol 75, 75:25–114, 2012.

[49] A. M. George and J. F. Stebbins. Structure and dynamics of magnesium in silicate melts: A high-temperature Mg-25 NMR study. American Mineralogist, 83(9-10):1022–1029, September 1998.

[50] Kenneth J. D. Mackenzie and Richard H. Meinhold. MAS NMR study of pentacoordinated magnesium in grandidierite. American Mineralogist, 82(5-6):479–482, May 1997.

[51] K. J. D. Mackenzie and R. H. Meinhold. Mg-25 Nuclear-Magnetic-Resonance Spectroscopy of Minerals and Related Inorganics - a Survey Study. American Mineralogist, 79(3-4):250–260, 1994.

[52] A. M. George and J. F. Stebbins. High-Temperature Na-23 Mas Nmr Data for Albite - Comparison to Chemical-Shift Models. American Mineralogist, 80(9-10):878–884, 1995.

[53] S. K. Lee and J. F. Stebbins. The structure of aluminosilicate glasses: High-resolution O-17 and Al-27 MAS and 3QMAS. Journal of Physical Chemistry B, 104(17):4091–4100, 2000.

[54] X. Y. Xue and J. F. Stebbins. Na-23 Nmr Chemical-Shifts and Local Na Coordination Environments in Silicate Crystals, Melts and Glasses. Physics and Chemistry of Minerals, 20(5):297–307, 1993.

[55] G. Engelhardt and D. Michel. High-Resolution Solid-State NMR of Silicates and Zeolites. John Wiley & Sons Ltd, Chichester, 1987.

[56] B. C. Bunker, R. J. Kirkpatrick, and R. K. Brow. Local-Structure of Alkaline-Earth Boroaluminate Crystals and Glasses .1., Crystal Chemical Concepts Structural Predictions and Comparisons to Known Crystal-Structures. Journal of the American Ceramic Society, 74(6):1425–1429, 1991.

[57] A. Quintas, T. Charpentier, O. Majerus, D. Caurant, J. L. Dussossoy, and P. Vermaut. NMR study of a rare-earth aluminoborosilicate glass with varying CaO-to-Na2O ratio. Applied Magnetic Resonance, 32(4):613–634, 2007.

[58] J. S. Wu and J. F. Stebbins. Effects of cation field strength on the structure of aluminoborosilicate glasses: High-resolution B-11, Al-27 and Na-23 MAS NMR. Journal of Non-Crystalline Solids, 355(9):556–562, 2009.

[59] Jean-Paul Amoureux, Christian Fernandez, and Stefan Steuernagel. ZFiltering in MQMAS NMR. Journal of Magnetic Resonance, Series A, 123(1):116–118, November 1996.

[60] D. Massiot, B. Touzo, D. Trumeau, J. P. Coutures, J. Virlet, P. Florian, and P. J. Grandinetti. Two-dimensional magic-angle spinning isotropic reconstruction sequences for quadrupolar nuclei. Solid State Nuclear Magnetic Resonance, 6(1):73–83, February 1996.

[61] Marko Bertmer, Lars Züchner, Jerry C. C. Chan, and Hellmut Eckert. Short and Medium Range Order in Sodium Aluminoborate Glasses. 2. Site Connectivities and Cation Distributions Studied by Rotational Echo Double Resonance NMR Spectroscopy. The Journal of Physical Chemistry B, 104(28):6541–6553, July 2000.

[62] Frédéric Angeli, Marina Gaillard, Patrick Jollivet, and Thibault Charpentier. Contribution of 43Ca MAS NMR for probing the structural configuration of calcium in glass. Chemical Physics Letters, 440(4):324–328, June 2007.

[63] Frédéric Angeli, Olivier Villain, Sophie Schuller, Thibault Charpentier, Dominique de Ligny, Lena Bressel, and Lothar Wondraczek. Effect of temperature and thermal history on borosilicate glass structure. Physical Review B, 85(5):054110, February 2012.

[64] Magali Magnin, Sophie Schuller, Cyrille Mercier, Julien Trébosc, Daniel Caurant, Odile Majérus, Frédéric Angéli, and Thibault Charpentier. Modification of Molybdenum Structural Environment in Borosilicate Glasses with Increasing Content of Boron and Calcium

Oxide by 95Mo MAS NMR. Journal of the American Ceramic Society, 94(12):4274–4282, 2011.

[65] Thibault Charpentier, Peter Kroll, and Francesco Mauri. First-Principles Nuclear Magnetic Resonance Structural Analysis of Vitreous Silica. Journal of Physical Chemistry C, 113(18):7917–7929, May 2009. WOS:000265687600067.

[66] T. M. Clark, P. J. Grandinetti, P. Florian, and J. F. Stebbins. Correlated structural distributions in silica glass. Physical Review B, 70(6):064202, August 2004. WOS:000223716300032.

[67] F. Angeli, M. Gaillard, P. Jollivet, and T. Charpentier. Influence of glass composition and alteration solution on leached silicate glass structure: A solid-state NMR investigation. Geochimica Et Cosmochimica Acta, 70(10):2577–2590, 2006.

[68] Anne Soleilhavoup, Jean-Marc Delaye, Frédéric Angeli, Daniel Caurant, and Thibault Charpentier. Contribution of first-principles calculations to multinuclear NMR analysis of borosilicate glasses. Magnetic Resonance in Chemistry, 48(S1):S159–S170, 2010.

[69] A. Veber, M. R. Cicconi, H. Reinfelder, and D. de Ligny. Combined Differential scanning calorimetry, Raman and Brillouin spectroscopies: A multiscale approach for materials investigation. Analytica Chimica Acta, 998:37–44, January 2018.

[70] T. Deschamps, C. Martinet, D. de Ligny, J. L. Bruneel, and B. Champagnon. Low-frequency Raman scattering under high pressure in diamond anvil cell: Experimental protocol and application to GeO2 and SiO2 boson peaks. Journal of Non-Crystalline Solids, 358(23):3156–3160, December 2012.

[71] James B. Murdoch, Jonathan F. Stebbins, and Ian S. E. Carmichael. High-resolution 29Si NMR study of silicate and aluminosilicate glasses: the effect of network-modifying cations. American Mineralogist, 70(3-4):332–343, April 1985.

[72] M. Magi, E. Lippmaa, A. Samoson, G. Engelhardt, and A. R. Grimmer. Solid-state high-resolution silicon-29 chemical shifts in silicates. The Journal of Physical Chemistry, 88(8):1518–1522, April 1984.

[73] T. Nanba, M. Nishimura, and Y. Miura. A theoretical interpretation of the chemical shift of Si-29 NMR peaks in alkali borosilicate glasses. Geochimica Et Cosmochimica Acta, 68(24):5103–5111, 2004.

[74] Lin-Shu Du and Jonathan F. Stebbins. Nature of Silicon-Boron Mixing in Sodium Borosilicate Glasses: A High-Resolution 11B and 17O NMR Study. The Journal of Physical Chemistry B, 107(37):10063–10076, 2003.

[75] J. Hopf, S. N. Kerisit, F. Angeli, T. Charpentier, J. P. Icenhower, B. P. McGrail, C. F. Windisch, S. D. Burton, and E. M. Pierce. Glass–water interaction: Effect of high-valence cations on glass structure and chemical durability. Geochimica et Cosmochimica Acta, 181:54–71, May 2016.

[76] Frederic Angeli, Thibault Charpentier, Patrick Jollivet, Dominique de Ligny, Michael Bergler, Alexander Veber, Stéphane Gin, and Hong Li. Effect of thermally induced structural disorder on the chemical durability of International Simple Glass. npj Materials Degradation, 2(1):31, September 2018.

[77] Lin-Shu Du and Jonathan F Stebbins. Solid-state NMR study of metastable immiscibility in alkali borosilicate glasses. Journal of Non-Crystalline Solids, 315(3):239–255, January 2003.

[78] G. Tricot. The structure of Pyrex® glass investigated by correlation NMR spectroscopy. Physical Chemistry Chemical Physics, 18(38):26764–26770, September 2016. Publisher: The Royal Society of Chemistry.

[79] H. Yamashita, K. Inoue, T. Nakajin, H. Inoue, and T. Maekawa. Nuclear magnetic resonance studies of 0.139MO (or M ' O-2)center dot 0.673SiO(2)center dot(0.188-x)Al2O3 center dot xB(2)O(3) (M = Mg, Ca, Sr and Ba, M '= Na and K) glasses. Journal of Non-Crystalline Solids, 331(1-3):128–136, 2003.

[80] Q. J. Zheng, M. Potuzak, J. C. Mauro, M. M. Smedskjaer, R. E. Youngman, and Y. Z. Yue. Composition-structure-property relationships in boroaluminosilicate glasses. Journal of Non-Crystalline Solids, 358(6-7):993–1002, 2012.

[81] F. Angeli, T. Charpentier, S. Gin, and J. C. Petit. 17O 3Q-MAS NMR characterization of a sodium aluminoborosilicate glass and its alteration gel. Chemical Physics Letters, 341(1):23–28, June 2001.

[82] E. Molieres, F. Angeli, P. Jollivet, S. Gin, T. Charpentier, O. Majerus, P. Barboux, D. de Ligny, and O. Spalla. Chemical Durability of Lanthanum-Enriched Borosilicate Glass. International Journal of Applied Glass Science, 4(4):383–394, December 2013.

[83] Elisa Gambuzzi, Alfonso Pedone, Maria Cristina Menziani, Frédéric Angeli, Pierre Florian, and Thibault

Charpentier. Calcium environment in silicate and aluminosilicate glasses probed by 43Ca MQMAS NMR experiments and MD-GIPAW calculations. Solid State Nuclear Magnetic Resonance, 68-69:31–36, June 2015.

[84] Kazuo Nakamoto. Infrared and Raman Spectra of Inorganic and Coordination Compounds. In Handbook of Vibrational Spectroscopy. American Cancer Society, 2006.

[85] B. Bunker, D. Tallant, R. Kirkpatrick, and G. L. Turner. Multinuclear nuclear magnetic resonance and Raman investigation of sodium borosilicate glass structures, 1990.

[86] Bjorn O. Mysen and John D. Frantz. Raman spectroscopy of silicate melts at magmatic temperatures: Na2O-SiO2, K2O-SiO2 and Li2O-SiO2 binary compositions in the temperature range 25–1475°C. Chemical Geology, 96(3):321–332, April 1992.

[87] Daniel Neuville, Dominique De Ligny, and Grant Henderson. Advances in Raman Spectroscopy Applied to Earth and Material Sciences. In Reviews in Mineralogy and Geochemistry, volume 78, pages 509–541. February 2014.

[88] Paul McMillan. Structural Studies of Silicate Glasses and Melts-Applications and Limitations of Raman Spectroscopy. American Mineralogist, 69:622–644, July 1984.

[89] N. Trcera, S. Rossano, and M. Tarrida. Structural study of Mg-bearing sodosilicate glasses by Raman spectroscopy. Journal of Raman Spectroscopy, 42(4):765–772, April 2011.

[90] B. Hehlen and D. R. Neuville. Raman Response of Network Modifier Cations in Alumino-Silicate Glasses. The Journal of Physical Chemistry B, 119(10):4093–4098, March 2015.

[91] Kohei Fukumi, Junji Hayakawa, and Toru Komiyama. Intensity of raman band in silicate glasses. Journal of Non-Crystalline Solids, 119(3):297–302, May 1990.

[92] D. Manara, A. Grandjean, and D. R. Neuville. Advances in understanding the structure of borosilicate glasses: A Raman spectroscopy study. American Mineralogist, 94(5-6):777–784, May 2009.

[93] Noriyoshi Shibata, Masaharu Horigudhi, and Takao Edahiro. Raman spectra of binary high-silica glasses and fibers containing GeO2, P2O5 and B2O3. Journal of Non-Crystalline Solids, 45(1):115–126, July 1981.

[94] W. L. Konijnendijk and J. M. Stevels. The structure of borosilicate glasses studied by Raman scattering. Journal of Non-Crystalline Solids, 20(2):193–224, March 1976.

[95] Tetsuji Yano, Noboru Kunimine, Shuichi Shibata, and Masayuki Yamane. Structural investigation of sodium borate glasses and melts by Raman spectroscopy. II. Conversion between BO4 and BO2O- units at high temperature. Journal of Non-Crystalline Solids, 321(3):147–156, July 2003.

[96] Tetsuji Yano, Noboru Kunimine, Shuichi Shibata, and Masayuki Yamane. Structural investigation of sodium borate glasses and melts by Raman spectroscopy.: I. Quantitative evaluation of structural units. Journal of Non-Crystalline Solids, 321(3):137–146, July 2003.

[97] Tetsuji Yano, Noboru Kunimine, Shuichi Shibata, and Masayuki Yamane. Structural investigation of sodium borate glasses and melts by Raman spectroscopy. III. Relation between the rearrangement of super-structures and the properties of glass. Journal of Non-Crystalline Solids, 321(3):157–168, July 2003.

[98] W. J. Dell, P. J. Bray, and S. Z. Xiao. B-11 Nmr-Studies and Structural Modeling of Na2o-B2o3-Sio2 Glasses of High Soda Content. Journal of Non-Crystalline Solids, 58(1):1–16, 1983.

[99] Y. H. Yun and P. J. Bray. Nuclear Magnetic-Resonance Studies of Glasses in System Na2o-B2o3-Sio2. Journal of Non-Crystalline Solids, 27(3):363–380, 1978.

[100] Y. H. Yun, S. A. Feller, and P. J. Bray. Correction and Addendum to Nuclear Magnetic-Resonance Studies of the Glasses in the System Na2o-B2o3-Sio2. Journal of Non-Crystalline Solids, 33(2):273–277, 1979.

[101] A. Quintas, O. Majerus, M. Lenoir, D. Caurant, K. Klementiev, and A. Webb. Effect of alkali and alkaline-earth cations on the neodymium environment in a rare-earth rich aluminoborosilicate glass. Journal of Non-Crystalline Solids, 354(2-9):98–104, 2008.

[102] A. Quintas, D. Caurant, O. Majérus, T. Charpentier, and J. L. Dussossoy. Effect of compositional variations on charge compensation of AlO4 and BO4 entities and on crystallization tendency of a rare-earth-rich aluminoborosilicate glass. Materials Research Bulletin, 44(9):1895–1898, September 2009.

[103] J. C. C. Chan, M. Bertmer, and H. Eckert. Site connectivities in amorphous materials studied by

double-resonance NMR of quadrupolar nuclei: High-resolution B-11 <-> Al-27 spectroscopy of aluminoborate glasses. Journal of the American Chemical Society, 121(22):5238–5248, 1999.

[104] Thibault Charpentier, Maria Cristina Menziani, and Alfonso Pedone. Computational simulations of solid state NMR spectra: a new era in structure determination of oxide glasses. RSC Advances, 3(27):10550–10578, June 2013. Publisher: The Royal Society of Chemistry.

[105] J. Schneider, V. R. Mastelaro, E. D. Zanotto, B. A. Shakhmatkin, N. M. Vedishcheva, A. C. Wright, and H. Panepucci. Q(n) distribution in stoichiometric silicate glasses: thermodynamic calculations and Si-29 high resolution NMR measurements. Journal of Non-Crystalline Solids, 325(1-3):164–178, 2003.

[106] C. C. Lin, S. F. Chen, L. G. Liu, and C. C. Li. Size effects of modifying cations on the structure and elastic properties of Na2O-MO-SiO2 glasses (M = Mg, Ca, Sr, Ba). Materials Chemistry and Physics, 123(2-3):569–580, 2010.

[107] Jeffrey R. Allwardt and Jonathan F. Stebbins. Ca-Mg and K-Mg mixing around non-bridging O atoms in silicate glasses: An investigation using 17O MAS and 3QMAS NMR. American Mineralogist, 89(5-6):777–784, May 2004.

[108] A Yamada, S Izumi, K Mitsuhara, S Yoshida, and J Matsuoka. Local structure of Mg in Na2O-MgO-B2O3 glasses. Memoirs of the SR Center Ritsumeikan University, (18):63–69, May 2016.

[109] Georges Calas, Laurent Cormier, Laurence Galoisy, Aline Ramos, and Stephanie Rossano. Chemical bonding and structural ordering of cations in silicate glasses. volume Université d'été CEA-VALRHO, pages 51–58. 1998.

□